



**HAL**  
open science

# Surface Protolysis and Its Kinetics Impact the Electrical Double Layer

Max F Döpke, Fenna Westerbaan van der Meij, Benoit Coasne, Remco Hartkamp

► **To cite this version:**

Max F Döpke, Fenna Westerbaan van der Meij, Benoit Coasne, Remco Hartkamp. Surface Protolysis and Its Kinetics Impact the Electrical Double Layer. *Physical Review Letters*, 2022, 128 (5), pp.056001. 10.1103/PhysRevLett.128.056001 . hal-03739177

**HAL Id: hal-03739177**

**<https://cnrs.hal.science/hal-03739177>**

Submitted on 27 Jul 2022

**HAL** is a multi-disciplinary open access archive for the deposit and dissemination of scientific research documents, whether they are published or not. The documents may come from teaching and research institutions in France or abroad, or from public or private research centers.

L'archive ouverte pluridisciplinaire **HAL**, est destinée au dépôt et à la diffusion de documents scientifiques de niveau recherche, publiés ou non, émanant des établissements d'enseignement et de recherche français ou étrangers, des laboratoires publics ou privés.

# Surface Protolysis and its Kinetics Impact the Electrical Double Layer

Max F. Döpke,<sup>1</sup> Fenna Westerbaan van der Meij,<sup>1</sup> Benoit Coasne,<sup>2</sup> and Remco Hartkamp<sup>1,\*</sup>

<sup>1</sup>*Process & Energy Department, Delft University of Technology,  
Leeghwaterstraat 39, 2628 CB Delft, The Netherlands*

<sup>2</sup>*Univ. Grenoble Alpes, CNRS, LIPhy, 38000 Grenoble, France*

(Dated: July 27, 2022)

Surface conductivity in the electrical double layer (EDL) is known to be affected by proton hopping/diffusion at solid-liquid interfaces. Yet, the role of surface protolysis and its kinetics on the thermodynamic and transport properties of the EDL are usually ignored as physical models consider static surfaces. Here, using a novel molecular dynamics method mimicking surface protolysis, we unveil the impact of such chemical events on the system’s response. Protolysis is found to strongly affect the EDL and electrokinetic aspects with major changes in  $\zeta$ -potential and electroosmotic flow.

Solid-liquid interfaces, which are omnipresent in nature, are central to many scientific fields such as colloid/materials science, phase separation/catalysis, and electrochemistry/energy harvesting. A detailed understanding of such interfaces is of paramount importance to design novel energy devices (e.g. batteries, osmotic power membranes) and innovative health/environment applications (e.g. drug delivery capsules, medium pollution/remediation). Solid-liquid interfaces are characterized by two parallel layers of equal charge and opposite polarity known as the electrical double layer (EDL) [1]. The electric charge distribution across these layers is usually described via mean-field models, which disregard the microscopic intricacies of the interfacial structure and chemistry. Beyond such pioneering approaches, researchers have proposed ways to effectively account for molecular details including ion-specific effects, microscopic correlations and surface charge localization. In contrast, despite its acknowledged interplay with the EDL, surface reactivity is not included in available frameworks. In particular, proton exchange at oxide-electrolyte interfaces, which directly influences hydrogen hopping/diffusion and, hence, surface conductivity [2, 3], is usually disregarded in modeling endeavors as it is implicitly assumed that surface charge distributions evolve too slowly to affect the interfacial fluid structure and dynamics.

Experimentally, proton exchange rates can only be measured from the interface transient response to an applied perturbation such as with pressure-jump techniques [4]. However, with most methods, only lower bounds or orders of magnitude can be estimated for such reaction rates. For instance, in atomic force microscopy experiments on silica with tip speeds as fast as  $0.5 \mu\text{m/s}$ , charge regulation due to the EDL overlap between the surface and tip is so fast that no hysteresis is observed in force-distance curves [5]. This suggests that surface chemistry adapts within milliseconds – a value consistent with flow experiments on mineral surfaces probing the electronic response induced by com-

position changes [6–8]. Dissolution experiments also provide lower bounds for protolysis rates. To form a  $\text{Si}(\text{OH})_4$  molecule from a  $\text{SiO}_4$  tetrahedron in  $\text{SiO}_2$ , multiple hydrolysis ( $\text{MOM} + \text{H}_2\text{O} \rightleftharpoons \text{MOH} + \text{MOH}$ ) and protolysis ( $\text{MOH} \rightleftharpoons \text{MO}^- + \text{H}^+$ ) reactions occur [9] (with protolysis being very fast and nearly activation-less compared to hydrolysis [10]). Dissolution rates of  $10^{-7} \text{mol/m}^2/\text{s}$  for silica under neutral pH, thus serve as a lower bound for surface protolysis rates [11, 12]. Despite such estimates, exact equilibrium protolysis rates and their influence on the EDL cannot be experimentally probed.

Theoretically, while first-principles calculations provide insights into reaction mechanisms, energy barriers and adsorption energies, the small system sizes in these approaches [ $O(10-100)$  atoms] are insufficient to study the fluid response [13–17]. On the other hand, classical molecular dynamics (MD) simulations [ $O(10^3 - 10^5)$  atoms] probe the fluid response, but they generally do not account for chemical reactions. Only recently, the computational power has increased to allow atomistic MD simulations to probe chemical reactions and fluid responses. In this context, the reactive force field ReaxFF [18] is an important landmark but parameters for protolysis are not available. In contrast, the dissociative force field MGFF [19, 20] allows reproducing OH bond dissociation/formation involved in proton reactions. Using this force field, when set in contact with water, protolysis rates up to  $2 \times 10^5 \text{mol/m}^2/\text{s}$  were found for hydroxylated silica surfaces containing strained sites ( $\text{Si}(\text{OH})\text{Si}$  and  $\text{SiOH}_2$  defects), while smaller rates between 900 and  $1750 \text{mol/m}^2/\text{s}$  were assessed when only considering silanol sites ( $\text{SiOH}$ ) [21, 22]. The OH bond lifetime was found to be broadly distributed from fs to ns with an average of the order of ps. Despite its ability to model silanol dissociation, the MGFF force field is unsuitable to study the impact of reaction kinetics on the EDL as ion parameters are not available.

In this letter, we first develop a novel framework to include surface reactions in classical MD simulations at no additional computational cost. This is achieved by adding every  $t_r$  time in the MD simulation a stochastic deprotonation/reprotonation step between two randomly

\* r.m.hartkamp@tudelft.nl

96 picked, independent surface sites (one protonated, one  
 97 deprotonated). Using this effective yet robust strategy,  
 98 we then investigate the impact of proton exchange and  
 99 its kinetics on the EDL formed in a prototypical silica-  
 100 electrolyte system. We find that both the ion distribu-  
 101 tion and dynamics within the EDL are strongly impacted  
 102 by proton exchange with significant effects on the sys-  
 103 tem’s electrokinetic response. By analyzing the molec-  
 104 ular mechanisms of ion diffusion within the EDL, we  
 105 unravel that ion adsorption times become much shorter  
 106 when surface protolysis is taken into account while the  
 107 water structure and dynamics are only indirectly im-  
 108 pacted through the electrostatic coupling with ions.

109 Using the LAMMPS package [23], we imple-  
 110 mented protonation/deprotonation reactions of the form  
 111  $\text{MOH} \rightleftharpoons \text{MO}^- + \text{H}^+$  in MD simulations by adjusting  
 112 the partial charges and Lennard-Jones parameters of a  
 113  $\text{MO}^-$  group to a  $\text{MOH}$  group and *vice versa*. As shown  
 114 in Fig. 1a, without explicitly forming or breaking OH  
 115 bonds, this strategy mimics equilibrium situations in  
 116 which no net adsorption or desorption takes place – pro-  
 117 tonation/deprotonation always occur simultaneously. In  
 118 doing so, direct proton exchange between  $\text{MOH}$  and  $\text{MO}^-$   
 119 sites avoids dealing with free protons and/or water ion-  
 120 ization reactions while maintaining a constant overall  
 121 surface charge. In principle, protonation and depro-  
 122 tonation could be treated as decoupled from each other  
 123 using a canceling background charge. However, the use  
 124 of concomitant protonation/deprotonation allows impos-  
 125 ing a thermodynamic ensemble with well-defined con-  
 126 stant parameters (surface charge, number of particles,  
 127 temperature, and overall charge neutrality). As shown  
 128 in Fig. 1c, various reaction rates  $r$  can be considered by  
 129 performing protonation/deprotonation at different time  
 130 intervals  $t_r \sim 1/r$  (see Tab. SI of the Supplemental Ma-  
 131 terial [24], upon decreasing  $t_r$ , the simulation time step  
 132 was decreased to ensure numerical stability). This im-  
 133 plementation does not account for mutual coupling be-  
 134 tween fluid structure and surface chemistry. In reality,  
 135 the probability to protonate/deprotonate a site depends  
 136 on its environment at a given time. In principle, these  
 137 probabilities can be calculated using for example reactive  
 138 force fields such as those cited above. However, calculat-  
 139 ing an instantaneous energy landscape on-the-fly leads  
 140 to prohibitive computational costs and statistical chal-  
 141 lenges. Moreover, including explicit water ionization re-  
 142 actions and water ions ( $10^{-6}$  mol/L for  $\text{H}^+/\text{H}_3\text{O}^+$  and  
 143  $10^{-8}$  mol/L for  $\text{OH}^-$  in bulk at neutral pH) is out of  
 144 reach (even for large MD systems like here, the num-  
 145 ber of water ions is too small to ensure statistical sig-  
 146 nificance). To circumvent such issues, we use here an  
 147 effective approach by stochastically selecting the surface  
 148 groups to react at a given time. With such a coarse-  
 149 grained description, we neglect (1) mechanisms occurring  
 150 on a time shorter than the chemistry timescale (1-10 fs),  
 151 (2) possible electric screening of surface sites by linger-  
 152 ing protons/hydroniums  $\text{H}^+/\text{H}_3\text{O}^+$  and (3) the fact that  
 153 protonation/deprotonation occur independently. These

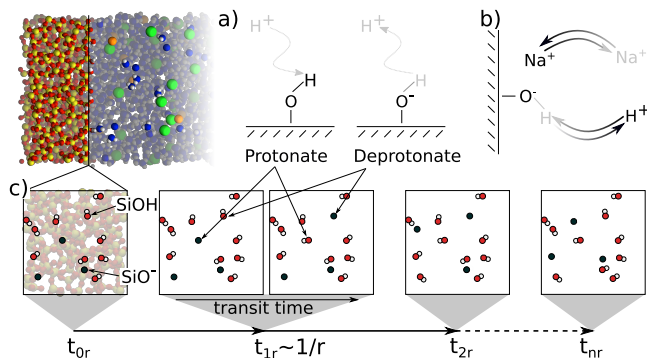


FIG. 1. a) Schematic view of protonation/deprotonation reactions at solid-liquid interfaces. Black font indicates interatomic interactions are turned on, while grey font indicates these are turned off. b) Protolysis reactions impact ion adsorption by allowing an ion to adsorb after site deprotonation (black) or forcing it to desorb after site protonation (grey). c) Simulation protocol flow diagram with time  $t_r \sim 1/r$  between protolysis reactions. Protonation/deprotonation events take place over a transit time to ensure numerical stability.

simplifications may result in overpredicting the impact of surface reactions but we expect such coarse-graining to be relevant as we only probe molecular events occurring in the EDL at longer times. Finally, to guarantee numerical stability, the parameter change between  $\text{MOH}$  and  $\text{MO}^-$  groups – which allows mimicking concomitant protonation/deprotonation – is linearly adjusted over 1 ps.

As a benchmark, we selected a prototypical amorphous silica slit pore of approximately 6 nm height filled with a 0.66-0.74 mol/L NaCl aqueous solution. Details on the set-up and force fields can be found in the Supplemental Material [24]. The reaction rate  $r$  was varied between no reactions (non-reactive MD, equivalent to  $r < 1.68$  mol/m<sup>2</sup>/s for our simulation size/time) and  $r = 10^4$  mol/m<sup>2</sup>/s. For reference, protolysis rates on silica-water interfaces were estimated in [21] to be of the order of  $10^2$ - $10^5$  mol/m<sup>2</sup>/s using dissociative MD. Given the surface area [12.4 nm<sup>2</sup>] and silanol density [4.7 SiOH/nm<sup>2</sup>] in our system, protonation/deprotonation take place between every >100 ns and 13.43 ps (see Tab. SI [24]). In comparison, as shown below,  $\text{Na}^+$  residence times are of the order of a few hundred ps so that we expect a non-negligible rate dependence.

Fig. 2a displays a typical cation density profile obtained in MD simulations of silica-electrolyte interfaces. Upon increasing the protolysis rate  $r$ , the cation peak in the density profile decreases, broadens and shifts away from the surface. These changes are consistent with a shift from predominantly specific to predominantly non-specific cation adsorption as demonstrated in Fig. S10a [24]. In other words, for large  $r$ , the average time for  $\text{Na}^+$  ions to adsorb may exceed the characteristic reprotonation time of a deprotonated site ( $\text{SiO}^-$  density/ $r$ , see Tab. SI [24]). From the cation perspective, the surface

charge effectively becomes more uniformly distributed as  $r$  increases. This results in the reduction of specifically adsorbed cations. As expected with less specific cation adsorption, anion adsorption is less pronounced (Fig. 2b) while water molecules are found to orient more strongly towards the surface (Fig. S5b [24]). Apart from this increased hydrophilicity,  $r$  is not found to impact the first solvation layer structure and water dynamics (Fig. S5 [24]). Fig. 2a also shows the parallel diffusion coefficients for cations (perpendicular diffusion coefficients are provided in Fig. S4 [24]). The methodology used to calculate such local diffusivities is described in Sec. SII [24]. These data show that faster desorption/adsorption and the reduction of specifically adsorbed cations, as induced by higher reaction rates  $r$ , lead to faster ion dynamics in the EDL. On the one hand, non-specifically adsorbed cations are more mobile, and on the other hand, as some cations quickly desorb from protonating  $\text{SiO}^-$  sites, other cations are attracted by deprotonating  $\text{SiOH}$  sites as illustrated in Fig. 1b. Consequently, upon increasing the protolysis rate  $r$ , the cation diffusion coefficients near the surface increase (inset in Figs. 2a and S4b [24]), while the average  $\text{Na}^+$  residence time decreases (Fig. 3). Since barely any anions specifically adsorb, their diffusion coefficients do not show any dependence on  $r$  (Figs. 2b and S4c [24]). Similarly, water diffusion coefficients and fluid viscosity are found to be nearly rate independent (Figs. S4a and S5(a,c) [24]).

Using the Boltzmann equation, the ion density profile can be written as  $\rho(\mathbf{x}) = \rho(\infty)\exp[-\beta\mathcal{F}_r(\mathbf{x})]$ , where  $\beta = 1/k_B T$ ,  $\rho(\infty)$  is the bulk density and  $\mathcal{F}_r(\mathbf{x})$  is the free energy landscape at a given rate  $r$ . Considering an energy landscape possessing different adsorption sites, the density profile in  $z$  follows  $\rho(z) = (L_x L_y)^{-1} \int \int \rho(\infty) \exp[-\beta\mathcal{F}_r(x, y, z)] dx dy$ , where the integrals run over the surface area. This expression can be considered in asymptotic limits depending on the reaction rate  $r$  and characteristic time  $\tau_e$  over which cations relax towards local equilibrium. For  $r\tau_e \ll 1$ , the surface can be considered “quenched” (non reactive). In this case, the surface contains a fraction  $\alpha_\bullet$  of protonated sites  $\text{MOH}$  and a fraction  $\alpha_o = 1 - \alpha_\bullet$  of deprotonated sites  $\text{MO}^-$  such that the density follows  $\rho(z) = \rho(\infty)\langle \exp[-\beta\mathcal{F}_r(z)] \rangle$ , where  $\exp[-\beta\mathcal{F}_r(z)] = \alpha_\bullet \exp[-\beta\mathcal{F}_\bullet(z)] + \alpha_o \exp[-\beta\mathcal{F}_o(z)]$ . For  $r\tau_e \gg 1$ , the surface can be considered “annealed” (reactive). In this case, all surface adsorption sites are equivalent since they frequently switch between protonated and deprotonated. The free energy of these equivalent sites is given by time average  $\beta\mathcal{F}_r(z) = \alpha_\bullet \beta\mathcal{F}_\bullet(z) + \alpha_o \beta\mathcal{F}_o(z)$  (we use ergodicity to replace the fraction of time spent in one site by its occurrence  $\alpha$ ). Assuming cations redistribute very fast according to the local free energy landscape, we can write the ion density as  $\rho(z) = \rho(\infty) \exp[-\beta\mathcal{F}_r(z)] = \rho(\infty) \exp[-\alpha_\bullet \beta\mathcal{F}_\bullet(z) - \alpha_o \beta\mathcal{F}_o(z)]$ . Provided proper boundary conditions are applied (surface charge and overall charge neutrality), these two limiting cases provide a framework to rationalize the simulated data. How-

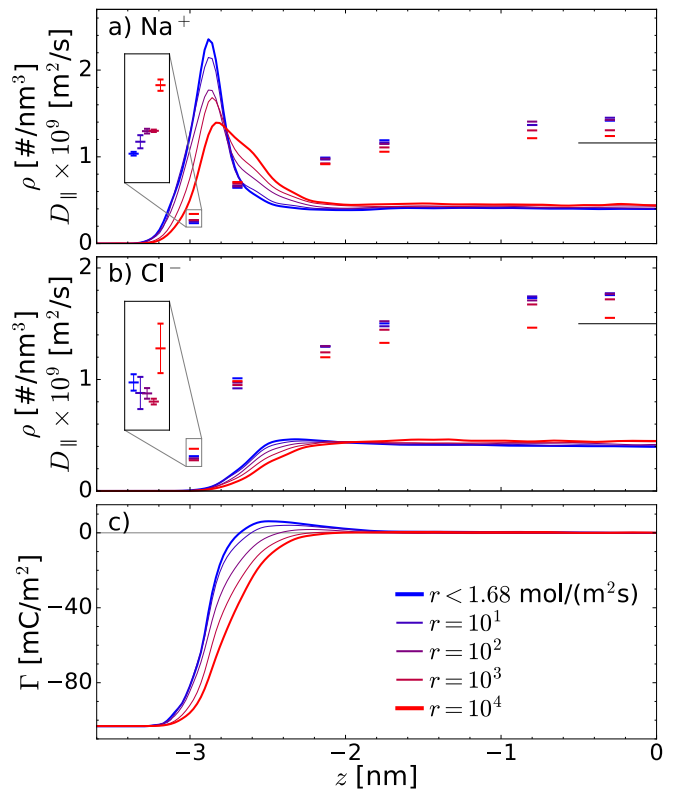


FIG. 2. a)  $\text{Na}^+$  and b)  $\text{Cl}^-$  density profiles (lines) and parallel diffusion coefficients (symbols). Symbols in the inset are shifted in  $z$  clarity. Black lines display the bulk diffusion coefficients obtained from independent bulk electrolyte simulations (see Fig. S6 [24]). c) Screening function  $\Gamma$ .  $z = 0$  is the channel center.

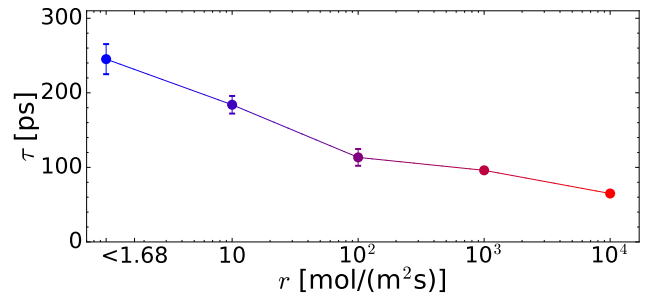


FIG. 3. Mean adsorption i.e. residence times,  $\tau = \int p_\tau dt$  (see Fig. S9 [24]) as a function of  $r$ .

ever, beyond such asymptotic cases, obtaining an expression for intermediate reactive rates  $r$  is not straightforward as in most situations the corresponding density profile cannot be written as a single contribution (annealed surface) nor as a weighted sum of two independent contributions (quenched surface). Indeed, in these situations, the observed density profile still derives from an underlying energy profile but proper averaging that leads to  $\rho(z)$  is ill-defined. In particular, in such intermediate situations, there is no clear time scale separation between the relaxation time towards local equilibrium and the typical

time between two protonation/deprotonation events so that one obtains density profiles that are rate dependent (in agreement with our simulation data). In the same spirit, one can see the observed density profile broadening as the result of an increased surface self-diffusivity  $D_s(z)$ . By writing that  $D_s(z)$  corresponds to the bulk diffusivity modulated by the surface/ion interaction, one predicts that the impact of reduced surface interactions due to protolysis reactions leads to a larger surface diffusivity [25]. In turn, such enhanced diffusivity leads to surface exploration corresponding to larger mean square displacements through the bulk phase between two relocations (re-adsorption), and hence, broader density profiles near the solid surface.

Upon increasing the reaction rate  $r$ , both ion densities increase in the channel center while the ion and water diffusion coefficients decrease (Figs. 2(a,b), S5a [24]). Although the EDL net charge is independent of  $r$ , the number of ions involved in the EDL decreases upon increasing  $r$ . In other words, cations and anions relocate in equal amounts from the EDL to the channel center as  $r$  increases. Such relocation would not notably affect bulk ion concentrations in a macroscopic channel. However, as shown in Fig. S1 [24], due to the small pore height  $H \approx 6$  nm (approximately 20 times the Debye length,  $\lambda_D \sim 0.35$  nm), a concentration increase from 0.66 to 0.74 mol/L can be detected when increasing  $r$  to  $10^4$  mol/m<sup>2</sup>/s. As a direct consequence of this concentration increase, the cation, anion and water diffusion coefficients in the channel center decrease. This is in agreement with data for bulk electrolyte simulations in Fig. S6 [24]. This finite channel size impact on ion concentration and diffusion is expected to become less pronounced as  $\lambda_D/H$  and/or  $r$  decrease.

The ion adsorption weakening observed upon increasing  $r$  also impacts the screening of the bare surface charge density  $\sigma_0$ . This can best be quantified by assessing the screening function  $\Gamma(z) = \sigma_0 + \int_{-\infty}^z e(\rho_{\text{Na}^+}(z') - \rho_{\text{Cl}^-}(z')) dz$ . As expected from the change from specific to non-specific adsorption upon increasing  $r$ , the screening peak in Fig. 2b shifts away from the surface and decreases in magnitude (the peak even disappears for the fastest rates). Surface reaction kinetics can, thus, directly impact the occurrence of charge inversion ( $\Gamma > 0$ ). This result can explain why many MD studies – carried out with a static surface charge distribution – report charge inversion under conditions for which no experimental charge inversion is found [26–28]. Another reason for such disagreement between MD and experiments may be force field shortcomings as investigated in our recent work [29].

We have thus far shown that reaction kinetics impacts ion adsorption, diffusion and screening of the bare surface charge. Based on these results, a strong impact of protolysis reactions on electrokinetic properties is expected. For example, the  $\zeta$ -potential in Fig. 4a is found to decrease with increasing reaction rate  $r$ . This result can be explained from changes in the ion density dis-

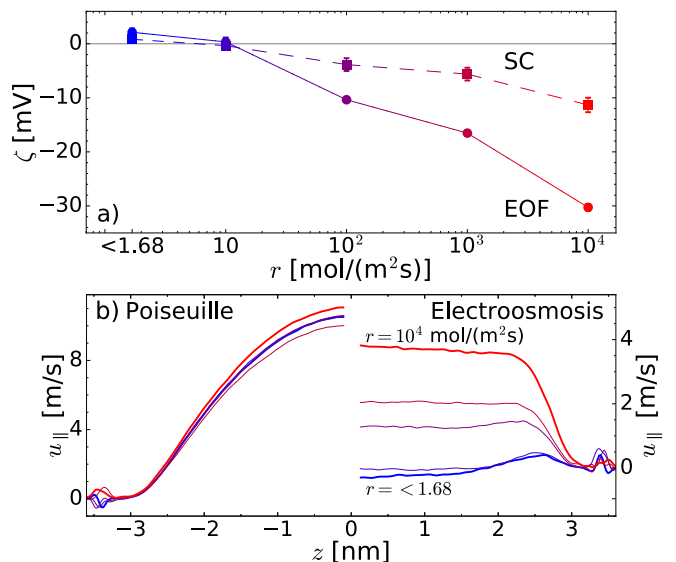


FIG. 4. a)  $\zeta$ -potential as a function of reaction rate  $r$  from streaming current (SC) and electroosmosis (EOF) simulations. b) Poiseuille (left) and electroosmosis (right) flow profiles resulting from a pressure drop of 75 atm and an electric field of 0.2 V/nm. These external forces have been shown to be within the linear response regime [28, 29].

tributions  $\rho_{\text{Na}^+}(z)$  and  $\rho_{\text{Cl}^-}(z)$  within the EDL (Figs. 2(a,b)). These distributions directly impact the streaming current  $I_{\text{str}} \sim \int e(\rho_{\text{Na}^+}(z') - \rho_{\text{Cl}^-}(z')) u_x dz$  and electroosmotic flow  $\eta \nabla^2 u_{\parallel}(z) = e(\rho_{\text{Na}^+}(z) - \rho_{\text{Cl}^-}(z)) E_x$ , which, in turn, fully determine the  $\zeta$ -potential through  $\zeta \sim I_{\text{str}}/\Delta p_x$  and  $\zeta \sim u_{\parallel, \text{bulk}}/E_x$  (following Helmholtz-Smoluchowski theory). Although the dependence of the  $\zeta$ -potential on the reaction kinetics in Fig. 4a appears to be stronger for electroosmosis than for streaming currents, the ion distributions corresponding to both methods are identical to those shown in Figs. 2(a,b). Hence, the differences in  $\zeta$ -potential between electroosmosis and streaming currents must originate from within the Helmholtz-Smoluchowski theory. In fact, in agreement with previous studies [29–31], these differences vanish when  $\zeta \rightarrow 0$ , which occurs at  $r = 10$  mol/m<sup>2</sup>/s. It is noteworthy that, since Poiseuille flow depends solely on fluid properties at the center of the channel, velocity profiles corresponding to the streaming currents are independent of  $r$  as shown in the left of Fig. 4b. Conversely, electroosmotic flow profiles, which are fully determined by the ion distribution within the EDL (following Navier-Stokes equation), change even qualitatively with  $r$  as shown in the right of Fig. 4b.

In summary, we developed a novel framework to account for surface reactions in classical MD simulations at no additional cost compared to non-reactive MD simulations. We then used this method to demonstrate that EDL properties and electrokinetic transport in a silica channel do not just depend on the static surface properties but also on proton exchange reaction kinetics. While such kinetic chemical events are not taken into consider-

ation in available formalisms, we provide strong evidence  
 that such processes affect static and dynamic proper-  
 ties of ions and solvent (water) within porous materials.  
 Specifically, upon increasing the surface reaction kinetics  
 (from no reactivity to rates encountered in experiments),  
 cation adsorption at the negatively charged surface be-  
 comes less pronounced with decreased retention times.  
 In turn, such decreased adsorption leads to increased lo-  
 cal diffusion coefficients near the solid surface. These  
 changes in ion distribution and dynamics within the EDL  
 also directly impact electrokinetic phenomena with – for  
 instance – the  $\zeta$ -potential reducing upon increasing the  
 protolysis reaction rate. The quantitative and qualita-  
 tive differences observed between non-reactive and reac-  
 tive surface charge distributions suggest that such equi-  
 librium surface reactions play an even more important  
 role for the EDL structure and dynamics than has thus  
 far been assumed. In fact, the impact of surface reactiv-  
 ity may even be more pronounced for surface groups with  
 weaker covalent bonds, at higher temperature, lower pH,  
 or for ions with longer residence times, questioning the  
 near-universal neglect of protolysis reactions in simula-  
 tion and modeling endeavours. Finally, our novel frame-  
 work provides a stepping stone for more realistic interface  
 modeling within a MD environment, potentially benefit-

ing applications ranging from the design of anti-corrosion  
 paints to electrochemical cells. Additional work should  
 also include establishing a bridge between our method  
 and fundamental approaches in which proton creation  
 and diffusion at surfaces is probed [32]. In this context,  
 mesoscopic strategies such as those based on the formal-  
 ism of intermittent Brownian motion applied to surface  
 adsorption and relocation in pores could prove useful in  
 linking molecular aspects and macroscopic observations  
 [25]. Moreover, to bridge the gap between the micro-  
 scopic and mesoscopic scales, the inclusion of water ion-  
 ization reactions from reactive simulations could provide  
 a means to account for chemical events occurring at the  
 fs time scale.

## ACKNOWLEDGMENTS

BC is grateful to Vivien Lecomte for the stimulating  
 discussion. This work was carried out on the Dutch na-  
 tional e-infrastructure with the support of SURF Coop-  
 erative. The scripts necessary to reproduce this work can  
 be found on GitLab [33].

- 
- [1] J. Lyklema, *Fundamentals of interface and colloid sci-  
 ence: soft colloids*, Vol. 5 (Elsevier, 2005).  
 [2] M. Nogami, R. Nagao, and C. Wong, *J. Phys. Chem. B*  
**102**, 5772 (1998).  
 [3] N. Amdursky, Y. Lin, N. Aho, and G. Groenhof, *Proc  
 Natl. Acad. Sci. U.S.A.* **116**, 2443 (2019).  
 [4] M. Ashida, M. Sasaki, H. Kan, T. Yasunaga, K. Hachiya  
 and T. Inoue, *J. Colloid Interface Sci.* **67**, 219 (1978).  
 [5] L. R. J. Scarratt, K. Kubiak, P. Maroni, G. Trefalt, and  
 M. Borkovec, *Langmuir* **36**, 14443 (2020).  
 [6] D. Lis, E. H. G. Backus, J. Hunger, S. H. Parekh, and  
 M. Bonn, *Science* **344**, 1138 (2014).  
 [7] B. L. Werkhoven, J. C. Everts, S. Samin, and R. van  
 Roij, *Phys. Rev. Lett.* **120**, 264502 (2018).  
 [8] P. Ober, W. Q. Boon, M. Dijkstra, E. H. Backus, R. van  
 Roij, and M. Bonn, *Nat. Commun.* **12**, 4102 (2021).  
 [9] M. Kagan, G. K. Lockwood, and S. H. Garofalini, *Phys  
 Chem. Chem. Phys.* **16**, 9294 (2014).  
 [10] B. M. Lowe, C.-K. Skylaris, and N. G. Green, *J. Colloid  
 Interface Sci.* **451**, 231 (2015).  
 [11] P. M. Dove and C. J. Nix, *Geochim. Cosmochim. Acta*  
**61**, 3329 (1997).  
 [12] S. A. Carroll, R. S. Maxwell, W. Bourcier, S. Martin, and  
 S. Hulse, *Geochim. Cosmochim. Acta* **66**, 913 (2002).  
 [13] M. Wilson and T. R. Walsh, *J. Chem. Phys.* **113**, 918  
 (2000).  
 [14] T. R. Walsh, M. Wilson, and A. P. Sutton, *J. Chem  
 Phys.* **113**, 9191 (2000).  
 [15] H.-P. Cheng, R. N. Barnett, and U. Landman, *J. Chem  
 Phys.* **116**, 9300 (2002).  
 [16] C. Mischler, J. Horbach, W. Kob, and K. Binder, *J  
 Phys.: Condens. Matter* **17**, 4005 (2005).  
 [17] Y.-W. Chen and H.-P. Cheng, *J. Chem. Phys.* **134**,  
 114703 (2011).  
 [18] A. C. T. van Duin, S. Dasgupta, F. Lorant, and W. A.  
 Goddard, *J. Phys. Chem. A* **105**, 9396 (2001).  
 [19] T. S. Mahadevan and S. H. Garofalini, *J. Phys. Chem. B*  
**111**, 8919 (2007).  
 [20] T. S. Mahadevan and S. H. Garofalini, *J. Phys. Chem. C*  
**112**, 1507 (2008).  
 [21] G. K. Lockwood and S. H. Garofalini, *J. Phys. Chem. C*  
**118**, 29750 (2014).  
 [22] T. S. Mahadevan and J. Du, *J. Am. Ceram. Soc.* **103**,  
 3676 (2020).  
 [23] S. Plimpton, *J. Comput. Phys.* **117**, 1 (1995).  
 [24] See Supplemental Material at [URL] for details on the  
 molecular dynamics simulations, theoretical framework  
 to calculate the local diffusion coefficients, details on the  
 electrokinetic theory and additional results..  
 [25] C. Bousige, P. Levitz, and B. Coasne, *Nat. Commun.* **12**,  
 1043 (2021).  
 [26] R. Hartkamp, B. Siboulet, J.-F. Duf r che, and B. Coasne,  
*Phys. Chem. Chem. Phys.* **17**, 24683 (2015).  
 [27] M. F. D pke, J. L tzenkirchen, O. A. Moulton, B. Si-  
 boulet, J.-F. Duf r che, J. T. Padding, and R. Hartkamp,  
*J. Phys. Chem. C* **123**, 16711 (2019).  
 [28] N. R. Haria and C. D. Lorenz, *J. Phys. Chem. C* **119**,  
 12298 (2015).  
 [29] M. F. D pke and R. Hartkamp, *J. Chem. Phys.* **154**,  
 094701 (2021).  
 [30] A. Szymczyk, P. Fievet, M. Mullet, J. Reggiani, and  
 J. Pagetti, *J. Membr. Sci.* **143**, 189 (1998).  
 [31] G. Hurwitz, G. R. Guillen, and E. M. Hoek, *J. Membr.  
 Sci.* **349**, 349 (2010).

- 457 [32] J. Comtet, B. Grosjean, E. Glushkov, A. Avsar, 461  
458 K. Watanabe, T. Taniguchi, R. Vuilleumier, M.-L. Boc-462  
459 quet, and A. Radenovic, Nat. Nanotechnol. **15**, 598  
460 (2020).
- [33] See Python and LAMMPS scripts at [<https://gitlab.com/mdopke/surfacereactions>].